

Supplementary Materials

**Conductivity boosted BiVO₄ for enhanced OER and supercapacitive performance:
Stability insights with modeling, predictions, and forecasting using machine learning
technique**

**Sagar A. Chaudhari¹, Vinod V. Patil¹, Vishal A. Jadhav¹, Parth Thorat², Santosh S. Sutar²,
Tukaram D. Dongale^{3,4}, Vinayak Parale⁵, Vaishali Patil⁶, Dattakumar S. Mhamane^{7,*},
Mukund G. Mali^{1,5,*}, Hyung-Ho Park^{5,*}**

¹School of Chemical Sciences, Punyashlok Ahilyadevi Holkar Solapur University, Solapur 413255, India.

²Yashwantrao Chavan School of Rural Development, Shivaji University, Kolhapur 416004, India.

³Computational Electronics and Nanoscience Research Laboratory, School of Nanoscience and Biotechnology, Shivaji University, Kolhapur 416004, India.

⁴Functional Materials and Materials Chemistry Laboratory, Department of Physiology, Saveetha Dental College & Hospitals, Saveetha Institute of Medical & Technical Sciences, Saveetha University, Chennai 600077, India.

⁵Department of Materials Science and Engineering, Yonsei University, Seoul 03722, Republic of Korea.

⁶Department of Engineering Sciences and Humanities, Vishwakarma Institute of Technology, Pune, Maharashtra 411048, India.

⁷Department of Chemistry, Sangameshwar College (Autonomous), Solapur 413001, India.

***Correspondence to:** Prof. Hyung-Ho Park, Department of Materials Science and Engineering, Yonsei University, 50 Yonsei-ro, Seodaemun-gu, Seoul 03722, Republic of Korea. E-mail: hhpark@yosei.ac.kr, Dr. Mukund G. Mali, School of Chemical Sciences, Punyashlok Ahilyadevi Holkar Solapur University, Solapur-Pune National Highway, Kegaon, Solapur 413255, India. E-mail: mukundgmali@gmail.com; Dr. Dattakumar S. Mhamane, Department of Chemistry,

Sangameshwar College (Autonomous), Solapur, 165, Railway Lines, Saat Rasta, Solapur
413001, India. E-mail: dkumar.mhamane@gmail.com

Section S1: Characterization and electrochemical measurements

S1.1- Structural and morphological characterizations:

The crystallinity of our catalyst is confirmed by an X-ray Diffractometer (Rigaku ultima-IVD/Max2500). The optical was studied using FTIR (Bruker Alpha II). Structure and surface morphology were determined by field emission-scanning electron microscopy with energy dispersive spectroscopy (FEI Nova Nano SEM 450). The microstructural investigations are examined through HRTEM (FEI, Titan G2 ChemiSTEM Cs Probe), and XPS analysis is used to examine the chemical states of elements in the catalyst (ULVAC-PHI Quantera SXM).

S1.2- Electrochemical measurements:

The electrodes were fabricated with well-polished SS substrates (1 cm × 5 cm pieces) they were ultrasonically processed 3 times in ethanol and DI water for further use as a substrate to deposit an electrocatalyst. The mixture of 80% active material, 15 % acetylene black, and 15 % polyvinylidene fluoride (PVDF) binder dissolved in N-methyl-2-pyrrolidone NMP solvent coated on SS substrates. OER performance was electrocatalytically analyzed on an Origalys electrochemical workstation utilizing a standard three-electrode electrochemical cell arrangement. An SS substrate coated with an electrocatalyst was used as a working electrode and a counter electrode platinum metal wire was incorporated, for the reference electrode the mercury/mercury oxide (Hg/HgO) filled with 1 M KOH was used. At room temperature, 1 M KOH electrolyte (pH=14) was employed to evaluate OER and supercapacitor performance. The LSV curves at 1 mV s⁻¹ scan rate were recorded in the potential window from 1 V to 1.675 V vs. RHE to calculate the overpotentials at the current density of 10 mA cm⁻². The electrochemical active surface area (ECSA) was measured by recording CV curves at different scan rates in the potential window of 0.92 to 1.22 vs. RHE. At 10 mV AC amplitude, the electrochemical impedance spectroscopy (EIS) was recorded within the frequency range of 1 MHz to 10 mHz. To investigate catalyst durability, a 12-hour chronoamperometry (CA) research at overpotential was performed on the best-performing material electrode. The electrochemical characteristics of the electrodes were investigated using Cyclic Voltammetry (CV), Galvanostatic Charge Discharge

(GCD), and Impedance Spectroscopy (EIS). The three-electrode system was used, where BVC and BV were working electrodes, Platinum wire was used as a counter electrode, and Hg/HgO was used as a reference electrode. The CV measurements at the scan rates from 100 to 10 mV s⁻¹ in the potential window of 0 to -1.0 V vs. Hg/HgO were measured in 1 M KOH as an electrolyte.

S1.3- Fabrication of symmetric supercapacitor devices:

BVC-coated SS films were used as the cathode (Positive) and anode (Negative) electrodes for the fabrication of symmetric supercapacitor devices. For the aqueous symmetric supercapacitor device, 1 M KOH solution was used as an electrolyte. Moreover, the symmetric solid-state supercapacitor device was fabricated using a 5×5 cm² area of positive and negative electrodes with PVA-KOH gel electrolyte. For the fabrication of a solid-state device, both electrodes were soaked with PVA-KOH electrolyte stacked on each other into the sandwich-like setup and pressed under 0.5-ton hydraulic pressure.

S1.4- Preparation of PVA–KOH gel electrolyte:

The process is as follows 3 gm of poly-vinyl alcohol (PVA) was dissolved in 30 mL of DDW by heating at 80°C for 2 hr. using continuous stirring mode. After the addition of PVA, freshly prepared 1 M KOH (10 ml) was added slowly to the solution and stirred at room temperature to form a transparent and viscous solution. To fabricate an all-solid-state symmetric supercapacitor, the prepared PVA-KOH gel was used as an electrolyte.

Section S2: Figures and tables

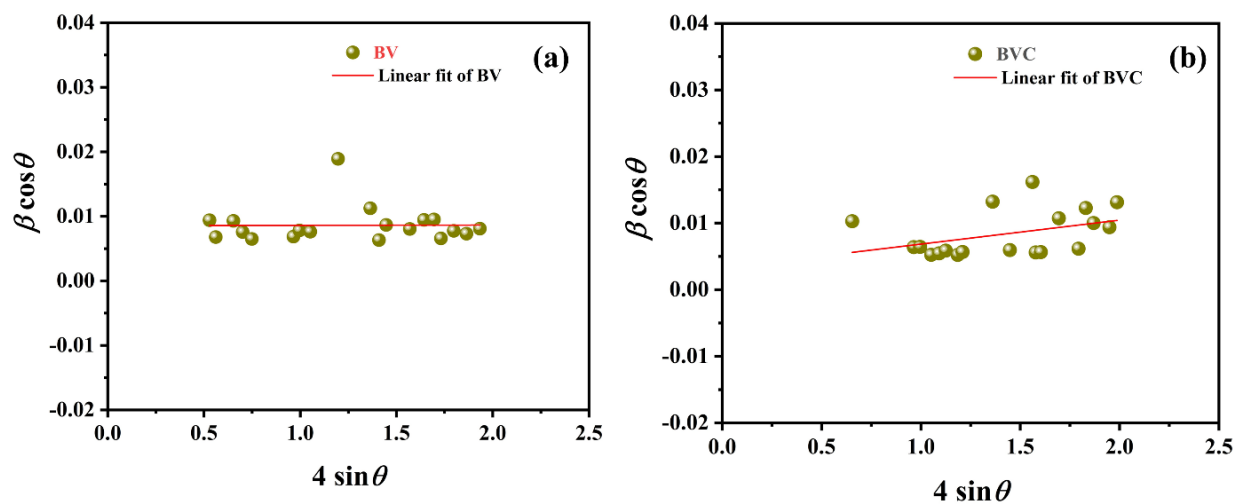


Figure S1. Williamson-Hall plots of (a) BV and (b) BVC samples.

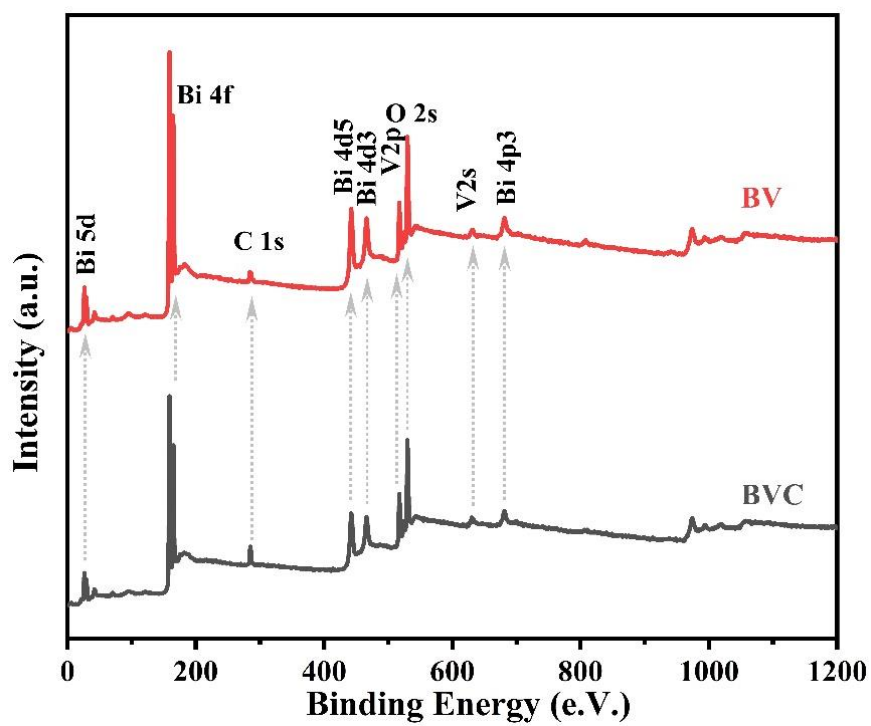


Figure S2. XPS survey spectrum of BV and BVC samples.

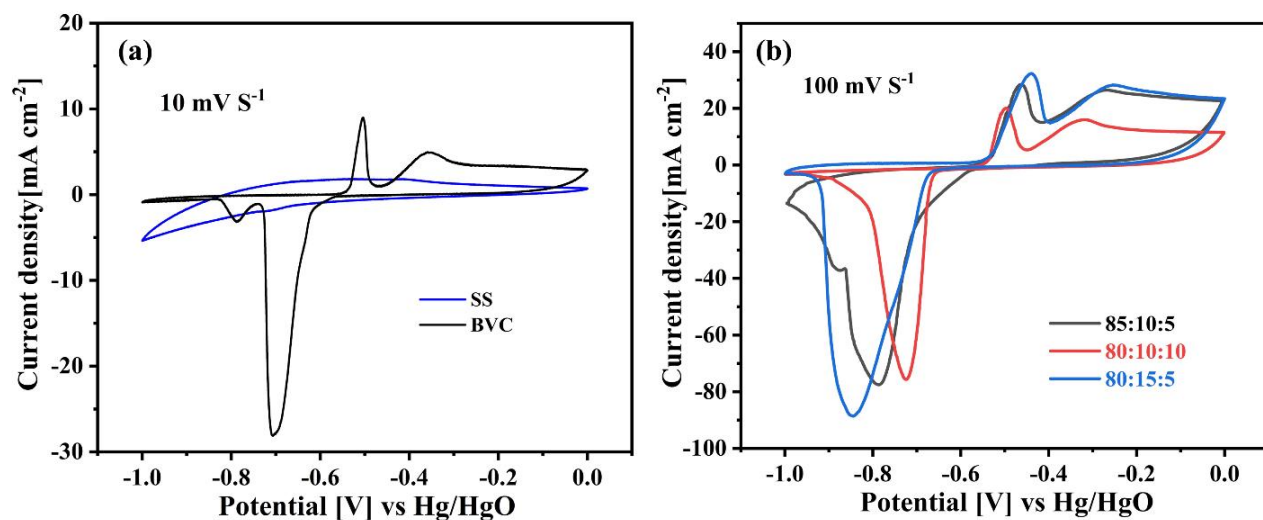


Figure S3. (a) Comparative CV curves of SS electrode, BV, and BVC at 10 mV S⁻¹ scan rate. (b) Comparative CV curves of BVC electrode with variation in active material, activated carbon, and PVDF at 100 mV S⁻¹ scan rate.

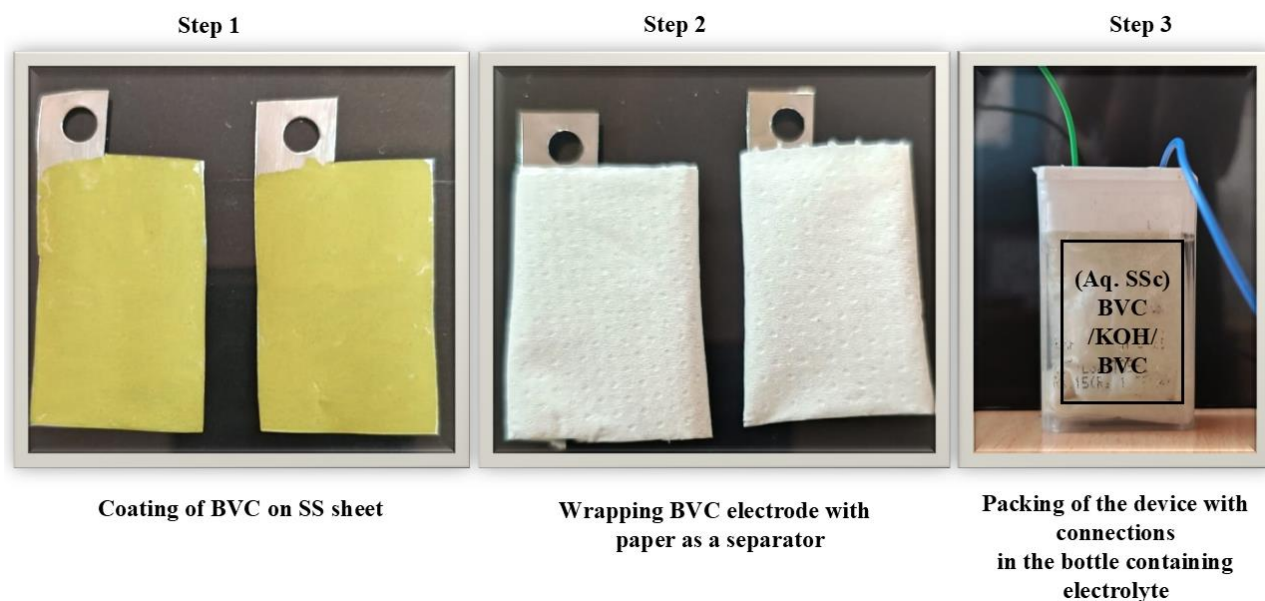


Figure S4. Photographs of steps involved in the fabrication of an aqueous device.

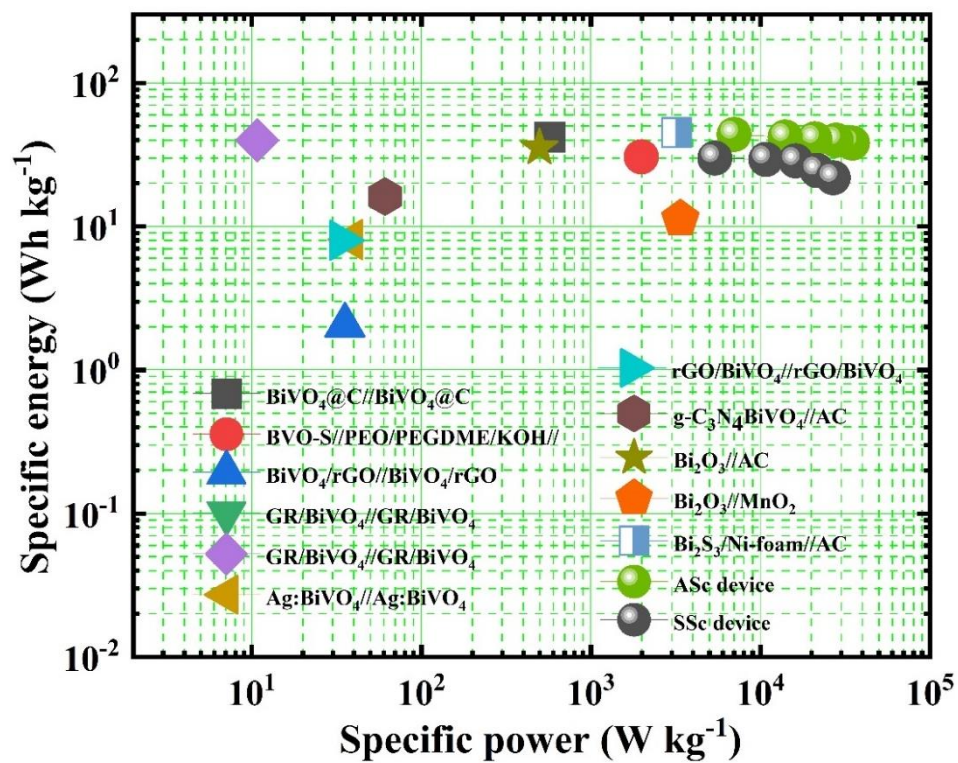


Figure S5. Ragone plot of SE and SP of the ASc and SSc device with current state of art.

Energy Materials

Table S1: XRD parameters of the samples

Sample Name	Angle (2 θ)	FWHM	Crystallite (Grain) size using Scherrer equation (nm)	Micro strain $\epsilon \times 10^{-3}$	Dislocation density (ρ) $\delta \times 10^{-3}$ (nm $^{-2}$)	Average Crystallite (Grain) size using Scherrer equation (nm)	Strain (ϵ) using W-H plot	Required crystallite size using W-H plot (nm)
BV	18.80 (110)	0.54012	14.908	14.235	4.499	17.11	0.0000410	16.197
BVC	18.83 (110)	0.59697	13.489	15.708	5.495	19.00	0.0036	42.662

Table S2: EIS fitted Values of the prepared samples

Materials	R_{ct} (Ω)	R_s (Ω)	R_w	CPE
BVC	0.07	0.018	0.367	0.101
BV	0.095	0.003	0.302	0.083
EIS fitted values of the BVC after stability				
After Stability BVC	2.43	0.85	0.456	0.012

Table S3: Performance comparison of BiVO₄ based supercapacitor

Electrode material	Synthesis method	Specific capacitance(F/g)	Capacitive retention	Electrolyte	Ref.
BiVO ₄ @C					
Flexible stainless steel mesh	SILAR	921.1 F/g@4 mA cm ⁻²	94.6% @5000 cycles	4 M KOH	[1]
BiVO ₄ @Ni foam	Sonochemical	214 F/g	70% @10,000 Cycles	3 M KOH	[2]
BiVO ₄ @GCE	Hydrothermal	1203F/g @ 2A/g	75% @2000 cycles	2 M KOH	[3]
Olive- BiVO ₄ Ni foam	Solvothermal	977F/g @ 0.5 A/g	86% @2000 cycles	1 M NaOH	[4]
BiVO ₄ @ SS substrate	SILAR	707@3 mV/s	102% @3500 cycles	1 M KCl	[5]
BiVO ₄ @ SS substrate	sol-gel	494.1 @5 mV/s	-	1M Na ₂ SO ₄	[6]
BiVO ₄ /PANI nickel foil	Hydrothermal	701F/g @ 1 A/g	95.4% @5000 cycles	1 M KOH	[7]
BiVO ₄ NPs-180°C Ni-foam	Hydrothermal	1451F/g @ 1 A/g	97.4% @5000 cycles	2 M KOH	[8]
BiVO ₄ @Ni foam	Hydrothermal	259.34@ 0.5 mA/g	-	-	[9]
BiVO ₄ nanocoral Ni foam	Hydrothermal	788 F/g@ 3 A/g	75% @1500 cycles	6 M KOH	[10]
BiVO ₄ @Ni foam	sol-gel	139 F/g@10 mV/s	-	2 M KOH	[11]
BiVO ₄ /rGO	Hydrothermal	400 F/g@5 mV/s	98% @1000 cycles	1 M Na ₂ SO ₄	[12]
BiVO ₄ nanorods Ni foam	Hydrothermal	1166F/g @ 1 A/g	80% @500 cycles	KOH	[13]

GR/BiVO ₄	Hydrothermal	479F/g @ 5	91% @2500	2 M	[14]
Ni foam		A/g	cycles	NaOH	
BiVO ₄ /RGO	Hydrothermal	343F/g @ 1	87% @2000	2 M	[15]
GCE		A/g	cycles	KOH	
MoS ₂ /BiVO ₄	Hydrothermal	610 F/g@ 1	80% @200	2 M	[16]
graphite plate		A/g	cycles	NaOH	
SWCNT/BiVO ₄	Solvothermal	395@2.5 A/g	88% @200	2 M	[17]
			cycles	NaOH	
Ag:BiVO ₄	Hydrothermal	170@5 mV/s	88% @4000 cycles	6M KOH	[18]
rGO/BiVO ₄	Hydrothermal	196@5 mV/s	-	6 M	[19]
carbon cloth				KOH	
BiVO₄@C	Solid state	483F/g @ 1	94% @2000	1 M	This
SS substrate		mA/g	cycles	KOH	

Table S4: MSE values of different models

Sr.No.	Parameter	MSE
1.	Current density (OER stability)	0.0008
2.	Capacitive retention of BVC	0.0222
3.	Coulombic efficiency of BVC	0.0038
4.	Capacitive retention of BV	0.0036
5.	Coulombic efficiency of BV	0.0046
6.	Capacitive retention of solid-state device	0.0010
7.	Capacitive retention of aqueous device	0.0013

Table S5: Rs and Rct Values of the prepared devices

Element	ASc device		SSc device	
	Before Stability	After Stability	Before Stability	After Stability
<i>R_s</i> (Ω)	0.39	0.41	0.11	0.13
<i>R_{ct}</i> (Ω)	92	210	96	276

<i>Rw</i>	0.0078	0.09	0.03	0.18
<i>CPE</i>	0.0034	0.00473	0.006	0.000381

Section S3: Formulas for calculations

S3.1- Formulas for XRD calculations:

Crystallite size, (D):

The crystallite size (nm) is calculated using the following Scherrer equation,²⁰

$$D = \frac{k \times \lambda}{\beta \times \cos \theta} \quad (\text{S1})$$

Where, k is the Scherrer constant, λ is the X-ray Wavelength, β is FWHM in radians, θ is the Bragg's angle.

Dislocation density (ρ_D), and Micro strain (ϵ):

The Micro strain (ϵ) and Dislocation density (ρ_D) were calculated using the following equations S1 and S2,^[20]

$$\epsilon = \frac{\beta_\gamma}{4 \tan[\text{rad}(\theta)]} \times 10^3 \quad (\text{S2})$$

$$\rho_D = \frac{1}{D^2} \times 10^3 \quad (\text{S3})$$

Strain (ϵ), and Required crystallite size (D):

The quantities of Strain (ϵ) and Required crystallite size (D) were also calculated from a linear least square fitting, namely Williamson–Hall plot analysis,^[21,22]

$$\beta \cos \theta = \frac{k \lambda}{D} = 4 \epsilon \sin \theta \quad (\text{S4})$$

From the slope and y-intercept of a plot of $4 \sin \theta$ versus $\beta \cos \theta$, one may determine the strain and crystallite size.

S3.2- Formulas for OER calculations:

RHE conversion (E_{RHE})

Voltages were converted from Hg/HgO to a reversible hydrogen electrode (RHE) by using the following equation

$$E_{\text{RHE}} = E_{\text{Hg} / \text{HgO}} + 0.059 \times \text{pH} + E_{\text{std}}. \quad (\text{S5})$$

Energy Materials

Where, E_{RHE} is voltage in terms of RHE and $E_{Hg/HgO}$ is potential in terms of the Hg/HgO electrode, pH is the pH of the electrolyte solution.

Over Potential

$$\eta_{10} = E_{RHE} - 1.23 \text{ V} \quad (\text{S6})$$

Where η_{10} is the overpotential measured at 10 mA cm⁻² current density, the value 1.23 V represents the theoretical minimum voltage required to split water, this is known as a thermodynamic potential for water splitting

Tafel slope

The Tafel plots were calculated by the equation

$$\eta = a + b \times \log|j| \quad (\text{S7})$$

where a , b , and j are the intercept, slope, and current density respectively.

Electrochemical double-layer capacitance (C_{dl})

The double-layer charging currents (i_c) can be plotted against the scan rate to determine the C_{dl} , using following

$$i_c = \nu C_{dl} \quad (\text{S8})$$

Where the scan rate is denoted by ν , it outputs a line that is straight and has a slope of C_{dl} .

Electrochemical active surface area (ECSA)

The ECSA was then calculated from the corresponding C_{dl} values. The material with a higher ECSA value displays a superior electrocatalytic activity.

$$\text{ECSA} = C_{dl} / C_s \quad (\text{S9})$$

Where, C_s is general specific capacity with a value of 0.04 mF cm⁻² of the alkaline 1.0 M KOH electrolyte solution.

Roughness factor (RF)

The electrocatalytic interface texture of electrodes, i.e. roughness factor, is calculated by the following formula.

$$RF = ECSA / A_{Geometric} \quad (S10)$$

Where, $A_{Geometric}$ is the electrode's geometric area in contact with the electrolyte, 1 cm^2 in the present study.

S3.3- Formulas for Supercapacitor calculations:

Charge contribution:

Capacitive and diffusion-controlled processes contribute to the total charge storage of the electrode, and according to Power's law, CV current is dependent on scan rate and can be expressed as follows,

$$i = av^b \quad (S11)$$

$$\log(i) = \log(a) + b \log(v) \quad (S12)$$

Where, i and v correspond to the current (A) and scan rate (V s^{-1}), respectively, while a and b are the arbitrary constant.

The peak current density (Q_t) contributions from the surface pseudocapacitive process ($Q_s - I_{surface}$) and the battery-like bulk process ($Q_d - I_{bulk}$) by the following modified powers law.

$$Q_t = Q_s + Q_d \quad (S13)$$

Where Q_t is the total stored charge, the Q_s is denoted for the charge stored at the material's surface, and Q_d is for the redox reactions.

The Q_s and Q_d values are calculated by the total voltammetric charge Q_t (Charge stores C g^{-1}) versus the reciprocal square root of the sweep rate plot.

$$Q_t = Q_s + kv^{-1/2} \quad (S14)$$

Where k is a constant and Q_s can be evaluated from the plot intercept.

Specific capacitance and specific capacity:

The specific capacitance and specific capacity are related to the supercapacitor performance. The quantity of electrical charge that a supercapacitor can hold per unit of mass is measured by its specific capacitance and capacity. Based on GCD characteristic curves, specific capacity of three electrodes and the specific capacitance of devices were measured using the following equations:

$$(\text{Three electrodes}) SC_{sp} = \frac{I \times \Delta t}{m} \quad (S15)$$

Energy Materials

$$(\text{Three electrodes}) \ C_{sp}(\text{mAh g}^{-1}) = \frac{SC_{sp} \times \Delta V}{3.6} \quad (\text{S16})$$

$$(\text{Two electrodes}) \ SCs = 4 \frac{I \times \Delta t}{\Delta V \times m} \quad (\text{S17})$$

Here, SC_{sp} represents the specific capacity (C g^{-1}) of the prepared material, I represent the discharge current density (mA cm^{-2}), Δt is the discharge time (s), ΔV is the potential window (V), and m represents the mass of active material (gm cm^{-2}).

Specific energy (SE), and Specific power (SP):

The performance of a supercapacitor for different applications is determined by its specific energy (S.E.) (Wh kg^{-1}) and specific power (S.P.) (W kg^{-1}), which are significant parameters.

The quantity of energy a supercapacitor can store per unit volume or mass is referred to as its specific energy, and the specific power indicates how fast energy is released. The specific energy and power of fabricated hybrid asymmetric supercapacitor devices are calculated from the GCD characteristic curves using the following equations respectively

$$S.E. = \frac{0.5 \times SCs \times (\Delta V)^2}{3.6} \quad (\text{S18})$$

$$S.P. = \frac{E \times 3600}{\Delta t} \quad (\text{S19})$$

Where, the $S.E.$ is specific energy, $S.P.$ is specific power, SCs represents specific capacitance, V represents the applied voltage of the fabricated device, and Δt indicates discharge time.

Capacitive retention, and Coulombic efficiency:

Capacitive retention refers to the capability of a supercapacitor device to maintain its storage capacity over many charging-discharging cycles. It measures the longstanding stability and reliability of the supercapacitor's performance. The coulombic efficiency (η) refers to the ratio of charging to discharging time, at equal charge and discharge current densities.

$$\text{Capacitive retention } (\%) = \frac{\text{Final capacitance value}}{\text{Initial capacitance value}} \times 100\% \quad (\text{S20})$$

$$\text{Coulombic efficiency } (\eta \%) = \frac{t_D}{t_C} \times 100\% \quad (\text{S21})$$

Where, t_D is the discharging time and t_C is charging time.

Section S4: Videos of OER and Supercapacitor

Video S1. The Oxygen gas evolution during the measurements of the OER study.

Video S2. The charging and discharging of the ASc device by rotating the fan.

Video S3. The charging and discharging of the SSc device by rotating the fan.

References:

1. Mane, S. A.; Moholkar, A. V.; Ghule, A. V. A Green Approach for Synthesis of an Efficient Nano Pebbles-like BiVO_4 @C Electrode for Supercapacitor Application. *Next Materials* **2023**, *1* (4), 100045. <https://doi.org/10.1016/j.nxmte.2023.100045>.
2. Subbiah, M.; Ansalin Gnana Sowndarya, A.; Sundaramurthy, A.; Venkatachalam, S.; Saravanan, N.; Pitchaimuthu, S.; Srinivasan, N. Tailoring Hierarchical BiVO_4 Sub-Micron Particles for Enhanced Cyclability in Asymmetric Supercapacitor. *J Energy Storage* **2023**, *71* (June), 108137. <https://doi.org/10.1016/j.est.2023.108137>.
3. Balachandran, S.; Karthikeyan, R.; Jothi, K. J.; Manimuthu, V.; Prakash, N.; Chen, Z.; Liang, T.; Hu, C.; Wang, F.; Yang, M. Fabrication of Flower-like Bismuth Vanadate Hierarchical Spheres for an Improved Supercapacitor Efficiency. *Mater Adv* **2022**, *3* (1), 254–264. <https://doi.org/10.1039/d1ma00810b>.
4. Dhanasekaran, T.; Yesuraj, J.; Narayanan, V.; Kim, K. Gradient Oxygen Vacancies in BiVO_4 Olive-Seeds Nanostructure for Electrochemical Supercapacitor Applications. *Mater Chem Phys* **2021**, *269* (March), 124737. <https://doi.org/10.1016/j.matchemphys.2021.124737>.
5. Bommineedi, L. K.; Pandit, B.; Sankapal, B. R. Spongy Nano Surface Architecture of Chemically Grown BiVO_4 : High-Capacitance Retentive Electrochemical Supercapacitor. *Int J Hydrogen Energy* **2021**, *46* (50), 25586–25595. <https://doi.org/10.1016/j.ijhydene.2021.05.057>.
6. Randive, S. G.; Kore, R. M.; Lokhande, B. J. Sol-Gel Synthesis and Supercapacitive Characterization of Bismuth Vanadate. *Journal of Nano- and Electronic Physics* **2020**, *12* (2), 2–5. [https://doi.org/10.21272/JNEP.12\(2\).02027](https://doi.org/10.21272/JNEP.12(2).02027).
7. Srinivasan, R.; Elaiyappillai, E.; Anandaraj, S.; Duvaragan, B. kumar; Johnson, P. M. Study on the Electrochemical Behavior of BiVO_4 /PANI Composite as a High Performance Supercapacitor Material with Excellent Cyclic Stability. *Journal of Electroanalytical Chemistry* **2020**, *861*, 113972. <https://doi.org/10.1016/j.jelechem.2020.113972>.

8. Packiaraj, R.; Venkatesh, K. S.; Devendran, P.; Bahadur, S. A.; Nallamuthu, N. Structural, Morphological and Electrochemical Studies of Nanostructured BiVO₄ for Supercapacitor Application. *Mater Sci Semicond Process* **2020**, *115* (April), 105122. <https://doi.org/10.1016/j.mssp.2020.105122>.
9. Isacfranklin, M.; Deepika, C.; Ravi, G.; Yuvakkumar, R.; Velauthapillai, D.; Saravanakumar, B. Nickel, Bismuth, and Cobalt Vanadium Oxides for Supercapacitor Applications. *Ceram Int* **2020**, *46* (18), 28206–28210. <https://doi.org/10.1016/j.ceramint.2020.07.320>.
10. Zan, G.; Wu, T.; Chen, H.; Dong, F.; Wu, Q. BiVO₄ Nanocoral Superstructures and Their Excellent Electrical/Optical Dual-Functions. *J Alloys Compd* **2021**, *852*, 157035. <https://doi.org/10.1016/j.jallcom.2020.157035>.
11. Packiaraj, R.; Venkatesh, K. S.; Devendran, P.; Bahadur, S. A.; Nallamuthu, N. Synthesis and Characterization of Sol-Gel Derived BiVO₄ Nanoparticles for Electrochemical Applications. *Int J Eng Adv Technol* **2019**, *9* (1S3), 390–393. <https://doi.org/10.35940/ijeat.a1189.1291s419>.
12. Dutta, S.; Pal, S.; De, S. Hydrothermally Synthesized BiVO₄-Reduced Graphene Oxide Nanocomposite as a High-Performance Supercapacitor Electrode with Excellent Cycle Stability. *New Journal of Chemistry* **2018**, *42* (12), 10161–10166. <https://doi.org/10.1039/c8nj00859k>.
13. Packiaraj, R.; Devendran, P.; Asath Bahadur, S.; Nallamuthu, N. Structural and Electrochemical Studies of Scheelite Type BiVO₄ Nanoparticles: Synthesis by Simple Hydrothermal Method. *Journal of Materials Science: Materials in Electronics* **2018**, *29* (15), 13265–13276. <https://doi.org/10.1007/s10854-018-9450-0>.
14. Deng, L.; Liu, J.; Ma, Z.; Fan, G.; Liu, Z. H. Free-Standing Graphene/Bismuth Vanadate Monolith Composite as a Binder-Free Electrode for Symmetrical Supercapacitors. *RSC Adv* **2018**, *8* (44), 24796–24804. <https://doi.org/10.1039/c8ra04200d>.
15. Sengottaiyan, C.; Kalam, N. A.; Jayavel, R.; Shrestha, R. G.; Subramani, T.; Sankar, S.; Hill, J. P.; Shrestha, L. K.; Ariga, K. BiVO₄/RGO Hybrid Nanostructure for High Performance Electrochemical Supercapacitor. *J Solid State Chem* **2019**, *269*, 409–418. <https://doi.org/10.1016/j.jssc.2018.10.011>.
16. Arora, Y.; Shah, A. P.; Battu, S.; Maliakkal, C. B.; Haram, S.; Bhattacharya, A.; Khushalani, D. Nanostructured MoS₂/BiVO₄ Composites for Energy Storage Applications. *Sci Rep* **2016**, *6* (October 2017). <https://doi.org/10.1038/srep36294>.

17. Khan, Z.; Bhattu, S.; Haram, S.; Khushalani, D. SWCNT/BiVO₄ Composites as Anode Materials for Supercapacitor Application. *RSC Adv* **2014**, 4 (33), 17378–17381. <https://doi.org/10.1039/c4ra01273a>.
18. Patil, S. S.; Dubal, D. P.; Tamboli, M. S.; Ambekar, J. D.; Kolekar, S. S.; Gomez-Romero, P.; Kale, B. B.; Patil, D. R. Ag:BiVO₄ Dendritic Hybrid-Architecture for High Energy Density Symmetric Supercapacitors. *J Mater Chem A Mater* **2016**, 4 (20), 7580–7584. <https://doi.org/10.1039/c6ta01980c>.
19. Patil, S. S.; Dubal, D. P.; Deonikar, V. G.; Tamboli, M. S.; Ambekar, J. D.; Gomez-Romero, P.; Kolekar, S. S.; Kale, B. B.; Patil, D. R. Fern-like RGO/BiVO₄ Hybrid Nanostructures for High-Energy Symmetric Supercapacitor. *ACS Appl Mater Interfaces* **2016**, 8 (46), 31602–31610. <https://doi.org/10.1021/acsami.6b08165>.
20. Mathad, S. N.; Jadhav, R. N.; Patil, N. D.; Puri, V. Structural and Mechanical Properties of Sr²⁺-Doped Bismuth Manganite Thick Films. *International Journal of Self-Propagating High-Temperature Synthesis* **2013**, 22 (4), 180–184. <https://doi.org/10.3103/S1061386213040018>.
21. S.Gandhad, S.; M.Patil, P.; Mathad, S. N.; V.Hublikar, L.; Jeergal, P. R.; Durgadsimi, S. U.; Pujar, R. B. Structural, Williamson-Hall Plot and Size-Strain Analysis of Mg_xNi_{1-x}Al_xFe₂O₄ Ferrites. *International Journal of Advanced Science and Engineering* **2019**, 5 (4), 1146–1153. <https://doi.org/10.29294/ijase.5.4.2019.1146-1153>.
22. Prabhu, Y. T.; Rao, K. V.; Kumar, V. S. S.; Kumari, B. S. X-Ray Analysis by Williamson-Hall and Size-Strain Plot Methods of ZnO Nanoparticles with Fuel Variation. *World Journal of Nano Science and Engineering* **2014**, 04 (01), 21–28. <https://doi.org/10.4236/wjnse.2014.41004>.